

GNC-Pose: Geometry-Aware GNC-PnP for Accurate 6D Pose Estimation

Xiujin Liu
 jeanliu@umich.edu

University of Michigan

Abstract. We present GNC-Pose, a fully learning-free monocular 6D object pose estimation pipeline for textured objects that combines rendering-based initialization, geometry-aware correspondence weighting, and robust GNC optimization. Starting from coarse 2D–3D correspondences obtained through feature matching and rendering-based alignment, our method builds upon the Graduated Non-Convexity (GNC) principle [33] and introduces a geometry-aware, cluster-based weighting mechanism that assigns robust per-point confidence based on the 3D structural consistency of the model. This geometric prior and weighting strategy significantly stabilizes the optimization under severe outlier contamination. A final LM refinement further improve accuracy. We tested GNC-Pose on The YCB Object and Model Set [4], despite requiring no learned features, training data, or category-specific priors, GNC-Pose achieves competitive accuracy compared with both learning-based and learning-free methods, and offers a simple, robust, and practical solution for learning-free 6D pose estimation.

Keywords: Graduated Non-Convexity · Multiview Geometry · Monocular 6D Pose Estimation.

1 Introduction

Accurately detecting rigid objects and estimating their 6D poses from RGB images alone remains a long-standing challenge in industrial manufacturing. Reliable pose estimation enables a wide range of downstream applications—including robotic grasping, manipulation, object tracking, and autonomous interaction in unstructured environments.

While deep learning has greatly advanced 6D pose estimation in recent years, providing powerful feature representations and improving robustness under challenging visual conditions. These methods still face several practical limitations. They typically require large amounts of annotated data, object-specific training, and careful domain adaptation to operate reliably in real-world scenarios. In contrast, learning-free pipelines have become an attractive alternative in scenarios where training is infeasible, owing to their generality, flexibility, and strong geometric interpretability. However, classic learning-free methods, which often

rely on hand-crafted feature matching followed by classical PnP or RANSAC-PnP [7], struggle under real-world conditions. Feature correspondences are frequently contaminated by severe outliers, texture variable regions, occlusion, and self-symmetry, causing unstable optimization and inaccurate poses. More recent robust estimators based on the Graduated Non-Convexity (GNC) principle [33] offer a mathematically grounded way to handle outliers, yet they are rarely integrated into a full end-to-end pipeline and typically assume uniformly weighted correspondences, ignoring the underlying 3D structure clue of the object.

In this paper, we propose GNC-Pose, a fully learning-free pipeline for monocular 6D object pose estimation for textured objects that integrates rendering-based initialization, feature matching, geometry-aware weighting, robust GNC optimization, and temporal refinement into a unified framework. Based on coarse correspondences obtained via sparse feature matching and rendering-based alignment, we introduce a geometry-aware cluster weighting module that analyzes the 3D distribution of model points through voxelized clustering. This module assigns robust per-point confidence scores based on structural consistency, effectively highlighting informative regions and suppressing ambiguous or symmetric surfaces. These geometry-driven confidences guide a GNC-based PnP optimizer, in which the non-convexity parameter is gradually annealed to reject outliers and stabilize convergence. A final LM refinement further polishes the estimate.

Based on our experiments, we demonstrate that GNC-Pose achieves competitive accuracy among both learning-based and learning-free methods while the pipeline requires no learned features, no training data, and no category-specific priors, making it deployable on any unseen textured object, as long as its CAD model is available.

Our contributions are summarized as follows:

1. A unified, fully learning-free pipeline for monocular 6D pose estimation integrating feature matching, rendering-based alignment, perspective-n-point, and GNC optimization.
2. A geometry-aware cluster-based weighting mechanism that assigns robust per-point confidence based on the 3D structural consistency of the CAD model.
3. A GNC-based PnP optimization framework that effectively handles heavy outliers via gradual convexity annealing.

We will release the code to the public once the paper is accepted.

2 Related Work

2.1 Learning-free 6D Pose Estimation

The Perspective- n -Point (PnP) problem has been extensively studied in computer vision, with early formulations such as EPnP [18], RPnP [21], and DLS [3] providing closed-form or iterative solutions under ideal correspondences. Robustification techniques, including RANSAC-based PnP variants [7] and iterative reweighted least squares (IRLS) [14], improve stability under outliers but still rely heavily on the quality of the initial correspondences. ICP [2] and its

point-to-plane or point-to-surface extensions further refine alignment when depth is available. Another line of work seeks to bypass training by exploiting synthetic rendering, local descriptors, and geometric matching. Earlier methods use SIFT(Scale-Invariant Feature Transform) or ORB(Oriented FAST + BRIEF) [11, 25] features combined with view-based object templates, while more recent approaches rely on synthetic depth or multiview rendering to build correspondence libraries for ICP, RANSAC-PnP, or pose voting [5, 30, 9, 15].

2.2 Learning-Based 6D Pose Estimation.

Deep neural networks have enabled significant advances in 6D pose estimation from RGB or RGB-D inputs. Early direct regression approaches such as PoseCNN [31] and CDPN [23] estimate poses or keypoints in an end-to-end fashion. Correspondence-based and refinement methods like PVNet [24], GDR-Net [29], and CosyPose [17] utilize dense feature learning, correspondence prediction, and multi-view fusion to achieve accuracy. More recent work further improves robustness and generalization, for example SO-Pose [6], which exploits self-occlusion cues for direct 6D pose regression from RGB, and FoundationPose [30], which use large-scale render-and-compare or foundation models to handle novel objects given only CAD models or a few reference images.

2.3 Robust Non-Convex Optimization and GNC.

Graduated non-convexity (GNC)[33] provides a principled approach for solving robust estimation problems by gradually transforming a convex surrogate into a non-convex objective. Originally developed for M-estimators such as Geman-McClure [20] and Welsch losses [14], GNC has been successfully applied in SLAM, point cloud registration, and geometric model fitting. [1, 27, 35, 32, 28] Recent works also explore non-convex formulations for rotation averaging, essential matrix estimation, and robust bundle adjustment. [36, 34, 16]

2.4 Gaps

Several gaps remain. Deep learning methods, have achieved impressive accuracy. However, these approaches require extensive training data, object-specific fine-tuning, or large foundation models. They often generalize poorly to unseen objects, rely on high-quality meshes, or demand GPU resources that limit deployment in robotics settings. Moreover, their behavior is less transparent, making debugging and failure analysis more difficult. Classical 6D pose estimation pipelines rely on geometric cues such as feature matching, PnP, ICP, or multi-view rendering. These methods have the advantage of being learning-free, object-agnostic, and fully interpretable, and can be applied to any new object as long as a CAD model is available. However, their performance is often significantly affected by imperfect correspondences, symmetries, occlusion, and noise in either the image or the CAD model. Without strong regularization or learned

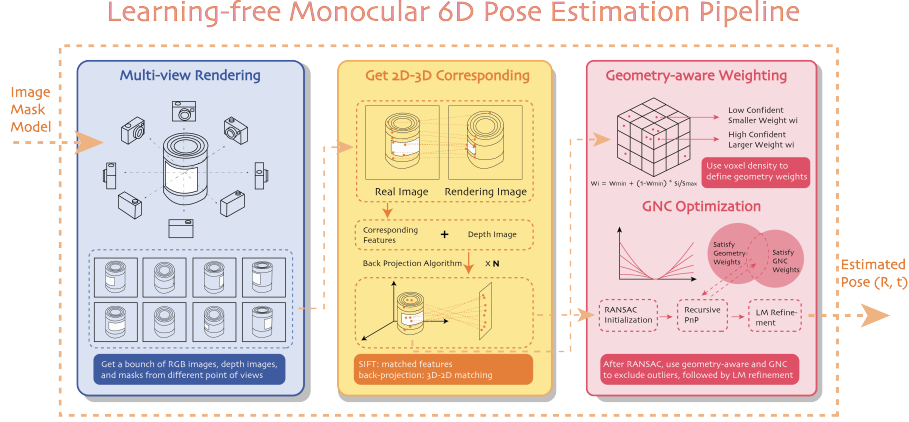


Fig. 1. Overall Pipeline of GNC-Pose: A fully learning-free 6D pose estimation pipeline for textured objects based on robust GNC-PnP optimization with structure-guided reweighting.

priors, classical pipelines tend to produce unstable inliers, degenerate PnP updates, or convergence to incorrect modes under ambiguity.

Bridging this gap requires methods that preserve the generality and interpretability of classical geometry-based pipelines while achieving robustness approaching that of learned models. Our work attempts to address this challenge by incorporating geometry-aware weighting and a graduated non-convexity PnP optimization scheme, enabling a fully learning-free pipeline to remain stable even under texture-variable regions, mismatching, and incomplete or inaccurate CAD geometry.

3 Methodology

3.1 Architecture

Figure. 1 depicts the structure of GNC-Pose. Given an input RGB image and the CAD model of the target object, the pipeline begins by performing a multi-view rendering sweep around the object model. By rendering the CAD model across an efficiently sampled set of azimuth and elevation angles, we obtain a library of synthetic silhouettes and projected key-points, providing rich geometric cues for coarse alignment. To address remain noisy due to occlusion, illumination changes, self-symmetry, and texture variation, GNC-Pose applies a geometry-aware clustering module, which voxelizes the 3D model and evaluates the structural consistency of each region. This produces per-point geometry-aware weights that emphasize discriminative geometric regions and down-weight ambiguous or symmetric surfaces. The weighted correspondences are then fed

into a GNC-based PnP optimizer, where the non-convexity parameter is gradually annealed to reject outliers and stabilize convergence. After GNC converges, a final LM-based refinement further [19] sharpens the pose estimate. This unified architecture enables GNC-Pose to operate reliably without learned features, training data, or category-specific priors, making it directly deployable on any new object given only its CAD model.

3.2 Geometry Aware Correspondence Weighting

To improve robustness under noisy correspondence generation, GNC-Pose introduces a geometry-aware correspondence weighting scheme that assigns each selected 3D point a confidence score derived from the structural characteristics of its local geometric neighborhood.

Given the set of sparse 2D–3D correspondences $\{(x_i, X_i)\}_{i=1}^N$, GNC-Pose constructs geometry-aware confidence weights by analyzing the spatial density of these viewpoint-dependent 3D points rather than the full CAD model. Each 3D point $X_i \in \mathbf{R}^3$ is first mapped into a discrete voxel grid of size v through $g_i = \lfloor X_i/v \rfloor \in \mathbf{Z}^3$, and points sharing the same voxel index implicitly form a local geometric cluster $\mathcal{C}_{g_i} = \{j \mid g_j = g_i\}$. The support count $s_i = |\mathcal{C}_{g_i}|$ serves as a discrete estimator of local matched-point density, approximating $\rho(X_i)v^3$ under sufficiently small v .

We then normalize the support values by the global maximum $s_{\max} = \max_j s_j$ to obtain $\hat{s}_i = s_i/s_{\max} \in [0, 1]$, and transform them into continuous geometry-aware weights

$$w_i = w_{\min} + (1 - w_{\min})\hat{s}_i,$$

ensuring $w_i \in [w_{\min}, 1]$. These weights reflect the structural reliability of each correspondence: dense, geometrically consistent regions receive $w_i \approx 1$, while isolated or noisy correspondences near edges or unstable surface regions are suppressed.

The resulting weights are integrated into the robust GNC-PnP formulation. Although the geometry-aware weights and the GNC scores resemble the multiplicative weighting used in classical IRLS formulations [14], GNC-Pose adopts them in a selection-based manner. Given the reprojection error $r_i(R, t) = \pi(K(RX_i + t)) - x_i^2$, we compute the Geman–McClure soft inlier score $w_i^{\text{gnc}}(\mu) = \frac{\mu^2}{r_i^2 + \mu^2}$, [33] which monotonically decreases with the residual magnitude. Combined with the geometry-aware prior w_i^{geom} , an inlier set is defined through

$$\mathcal{I}(\mu) = \{i \mid w_i^{\text{gnc}}(\mu) > \tau_{\text{gnc}} \wedge w_i^{\text{geom}} > \tau_{\text{geom}}\},$$

where τ_{gnc} and τ_{geom} are fixed thresholds.

Rather than entering a weighted normal equation, these weights determine which correspondences are retained at each GNC stage. The pose is then estimated by $\min_{R,t} \sum_{i \in \mathcal{I}(\mu)} \|\pi(K(RX_i + t)) - x_i\|^2$ via a standard iterative PnP solver. As μ decreases, the GNC score becomes increasingly selective, driving $w_i^{\text{gnc}}(\mu) \rightarrow 0$ for high-residual outliers, while the geometry-aware threshold suppresses correspondences arising from structurally unreliable regions.

3.3 GNC-Based PnP with Geometry-Aware Inlier Selection

Given the geometry-aware correspondences from Sec. 3.2, we estimate the object pose by minimizing a robust reprojection objective using a Graduated Non-Convexity (GNC) scheme. For each correspondence (x_i, X_i) , we define the squared reprojection residual

$$r_i(R, t) = \|\pi(K(RX_i + t)) - x_i\|^2,$$

and adopt the Geman–McClure M-estimator, whose GNC surrogate takes the form

$$\rho_\mu(r) = \frac{r}{r + \mu},$$

where $\mu > 0$ controls the non-convexity of the loss, as the underlying robust penalty. When μ is large, $\rho_\mu(r) \approx r/\mu$ is nearly convex and behaves similarly to a scaled ℓ_2 loss; as $\mu \rightarrow 0$, the penalty becomes strongly re-descending and approaches a truncated cost that saturates for large residuals.

The associated influence function

$$\psi_\mu(r) = \frac{\partial \rho_\mu(r)}{\partial r} = \frac{\mu}{(r + \mu)^2}$$

reveals that the contribution of a sample with residual r vanishes as r grows, and that decreasing μ makes this transition sharper. In the limit $\mu \rightarrow 0$, $\psi_\mu(r) \rightarrow 0$ for all $r > 0$, i.e., only exact inliers retain non-zero influence.

GNC implements this continuation principle by optimizing a sequence of surrogate problems with gradually decreasing μ . For optimization, instead of using $\psi_\mu(r)$ explicitly, we employ the standard Geman–McClure soft inlier score, for a fixed μ , we define a GNC soft inlier score

$$w_i^{\text{gnc}}(\mu) = \frac{\mu^2}{r_i^2 + \mu^2},$$

which is monotonically decreasing in r_i and behaves as a smooth soft-thresholding function: $w_i^{\text{gnc}}(\mu) \rightarrow 1$ when $r_i \ll \mu$ and $w_i^{\text{gnc}}(\mu) \rightarrow 0$ when $r_i \gg \mu$. In a conventional IRLS interpretation, such weights would modulate each correspondence’s contribution to a weighted normal equation. Rather than using them as continuous weights, GNC-Pose combine them with our geometry-aware structural prior w_i^{geom} to form a correspondence-selection rule $\mathcal{I}(\mu) = \{i \mid w_i^{\text{gnc}}(\mu) > \tau_{\text{gnc}} \wedge w_i^{\text{geom}} > \tau_{\text{geom}}\}$. This discrete selection mechanism mirrors the behavior of a re-descending M-estimator whose effective shape sharpens as μ decreases: for large μ , almost all correspondences satisfy the inequality and the objective behaves close to least squares; as μ becomes small, only points with both small residuals and reliable geometry survive, mimicking a re-descending loss with hard outlier rejection.

Algorithmically, we alternate between updating the inlier set $\mathcal{I}(\mu)$ and solving an weighted PnP on this set. Starting from an initial pose obtained by `solvePnP``Ransac`, we compute residuals r_i and set

$$\mu_0 = \kappa \cdot \text{median}_i(r_i) + \varepsilon,$$

Algorithm 1 GNC-PnP with Geometry-Aware Inlier Selection**Require:** 2D–3D correspondences $\{(x_i, X_i)\}$, intrinsics K , geometry weights w_i^{geom} .**Ensure:** Final pose (R, t) , inlier mask \mathcal{I} .

```

1:  $(R, t) \leftarrow \text{PnPRANSAC}$ 
2: Compute  $r_i = \|\pi(K(RX_i + t)) - x_i\|^2$ 
3:  $\mu \leftarrow k \cdot \text{median}(r_i) + \varepsilon$ 
4: repeat
5:    $w_i^{\text{gnc}} \leftarrow \mu^2 / (r_i^2 + \mu^2)$ 
6:    $\mathcal{I} \leftarrow \{i \mid w_i^{\text{gnc}} > \tau_{\text{gnc}} \wedge w_i^{\text{geom}} > \tau_{\text{geom}}\}$ 
7:   if  $|\mathcal{I}| < \text{min\_inliers}$  then
8:     break
9:   end if
10:   $(R, t) \leftarrow \text{solvePnP}(X_{\mathcal{I}}, x_{\mathcal{I}}; K, R, t)$ 
11:  Recompute  $r_i$ 
12:   $\mu \leftarrow \max(\gamma\mu, \mu_{\text{final}})$ 
13: until  $\mu \leq \mu_{\text{final}}$ 
14:  $(R, t) \leftarrow \text{solvePnPRefineLM}(X_{\mathcal{I}}, x_{\mathcal{I}}; K, R, t)$ 

```

where κ is a scaling factor that determines how close the initial GNC stage remains to a convex regime. A larger κ yields a more conservative (nearly convex) initialization with broader soft inlier acceptance, while a smaller κ initiates the optimization with sharper non-convexity and more aggressive outlier suppression. In practice, κ is chosen in the range $[3, 10]$ depending on the expected noise level of the initial correspondences.

We then iterate the following steps:

- (i) evaluate $w_i^{\text{gnc}}(\mu)$ for all correspondences;
- (ii) form the inlier set $\mathcal{I}(\mu)$ using the GNC and geometry thresholds;
- (iii) if $|\mathcal{I}(\mu)|$ is above a minimum inlier count, update (R, t) by running `solvePnP` with `SOLVEPNP_ITERATIVE` on the restricted set;
- (iv) recompute residuals and decrease μ according to

$$\mu \leftarrow \max(\gamma\mu, \mu_{\text{final}}), \quad 0 < \gamma < 1.$$

As μ is annealed, the inlier set monotonically contracts and the surrogate objective increasingly approximates the target non-convex M-estimator. When μ reaches its final value or convergence is detected, we perform a last local refinement using `solvePnPRefineLM` on the final inlier set. The complete procedure is summarized in Algorithm 1. Despite relying on a standard least-squares PnP solver in the inner loop, the outer GNC schedule and geometry-aware selection implement a principled non-convex robust optimization scheme that yields stable convergence under severe noise, occlusion, and correspondence outliers.

4 Experiment

We evaluate GNC-Pose on The YCB Object and Model Set [4]. Our experiments assess accuracy, robustness to outliers, and generalization to unseen objects.

Unless otherwise stated, all results are obtained without any training, using only the CAD model of the target object.

4.1 Dataset

We evaluate GNC-Pose on The YCB Object and Model Set [4]. The YCB Object and Model Set is one of the most widely used benchmarks for 6D pose estimation, providing a curated collection of household objects with accurate, high-resolution 3D meshes. The objects span a broad spectrum of geometric and photometric difficulty—including textureless surfaces, specular materials, and repetitive patterns, making the dataset well suited for evaluating correspondence robustness and pose stability.

In our experiments, we select a subset of 12 objects from the YCB Object and Model Set, focusing specifically on those with rich and distinctive textures. These objects provide more reliable visual cues for correspondence matching and thus offer a suitable testbed for assessing the robustness and accuracy of our 6D pose estimation pipeline.

4.2 Baseline

Our baselines cover the major paradigms of 6D pose estimation, including supervised detection-and-regression (PoseCNN [31]), dense correspondence matching (LoFTR [26]), supervised RGB-only refinement (DeepIM [22]), and learning-free Template Matching (TP-UB).

PoseCNN [31] is a foundational learning-based method for object pose estimation that directly regresses 6D pose from RGB images. Despite its strong supervised performance, PoseCNN requires extensive annotated training data and category-specific learning, making it a natural contrast to our fully learning-free formulation.

LoFTR [26] removes the need for a feature detector and instead applies Transformer self-attention and cross-attention to directly compute dense and robust matches between two images.

DeepIM [22] is another learning-based method. It is an RGB-based iterative pose refinement method that improves an initial 6DoF estimate by repeatedly predicting relative pose updates between the rendered object and the observed image.

Template matching approaches [8, 12] convert discrete pose estimation into a classification task by rendering thousands of CAD-based templates and retrieving the closest match. Following [10], our setting removes the reliance on accurate CAD models, and collecting and storing large numbers of support images is prohibitively costly. To approximate the upper bound of such methods, we assign the view whose rotation is closest to the ground truth and derive the translation from the center shift.

Together, these baselines cover the spectrum from supervised deep learning to classical geometry-driven methods, from correspondence matching to template

matching, enabling a comprehensive evaluation of the strengths and limitations of GNC-Pose.

4.3 Implementation Details

All experiments are performed on a MacBook Pro equipped with an Apple M2 Pro CPU without any GPU acceleration.

For each object, we randomly select 120 test images and exclude top-down views, which contain almost no distinctive features for reliable matching.

To build a coarse alignment database, we render synthetic views of the CAD model by sweeping azimuth from -180° to 180° at a fixed camera height of 1 m, producing silhouettes and projected keypoints for coarse alignment. Given an input RGB image, SIFT features are extracted and matched to the rendered views, Geometry-aware weights are computed by voxelizing the CAD model with a 5 mm grid and normalizing the local support density. We initialize the pose using `solvePnPRansac`, then apply our GNC-PnP refinement with $\mu_0 = 5 \cdot \text{median}(r_i)$, decay factor $\gamma = 0.5$, and final value $\mu_{\text{final}} = 0.5$. A final `solvePnPRefineLM` step further improves the pose estimate.

The complete pipeline requires no training data or category-specific priors.

4.4 Evaluation Metrics

For evaluation, we calculate the ADD and ADD-S AUC [31]. This corresponds to the area under the accuracy-threshold curve produced by varying the distance threshold. The maximum threshold is set to 10cm.

The standard Average Distance Deviation (ADD) metric [13] is used to measure the mean point-wise distance between object vertices transformed by the predicted pose $[R, t]$ and those transformed by the ground-truth pose $[\hat{R}, \hat{t}]$:

$$ADD = \frac{1}{m} \sum_{x \in M} \left\| (Rx + t) - (\hat{R}x + \hat{t}) \right\|.$$

where x is a vertex of totally m vertexes on the object mesh M . The ADD-S metric is intended for symmetric objects and defines the average distance based on nearest-neighbor point correspondences:

$$ADD_S = \frac{1}{m} \sum_{x_1 \in M} \min_{x_2 \in M} \left\| (Rx_1 + t) - (\hat{R}x_2 + \hat{t}) \right\|.$$

4.5 Qualitative Results

Table 1 summarized the results on YCB Object and Model Set [4]. The experimental results demonstrate that our method delivers a decisive performance advantage over non-deep-learning approaches, establishing a new benchmark for purely geometric pipelines. While state-of-the-art deep learning methods

Table 1. Quantitative evaluation of different 6D pose estimation baselines (TP-UB: upper bound of template approaches).

learning-free Object	PoseCNN [31]		LoFTR [26]		DeepIM [22]		TP-UB		Ours	
	\times ADDS	ADD	\times ADDS	ADD	\times ADDS	ADD	\checkmark ADDS	ADD	\checkmark ADDS	ADD
002_master_chef_can	84.0	50.9	87.2	50.6	93.1	71.2	62.2	21.4	<u>92.1</u>	51.3
003_cracker_box	<u>76.9</u>	51.7	71.8	25.5	91.0	83.6	65.6	5.0	75.0	68.9
004_sugar_box	<u>84.3</u>	68.6	63.9	13.4	96.2	94.1	66.7	21.5	69.2	50.0
005_tomato_soup_can	80.9	66.0	77.1	52.9	<u>92.4</u>	86.1	75.2	43.1	93.7	87.1
006_mustard_bottle	90.2	79.9	84.5	59.0	<u>95.1</u>	91.5	47.1	4.0	96.4	93.6
007_tuna_fish_can	<u>87.9</u>	70.4	72.6	55.7	96.1	87.7	72.8	38.4	83.2	70.4
008_pudding_box	79.0	62.9	86.5	68.1	90.7	82.7	<u>86.3</u>	18.4	83.2	72.8
009_gelatin_box	87.1	75.2	71.6	45.2	94.3	91.9	<u>90.9</u>	43.2	86.6	78.4
010_potted_meat_can	78.5	59.6	67.4	45.1	<u>86.4</u>	76.2	59.8	28.9	90.8	80.7
021_bleach_cleanser	71.9	50.5	36.9	16.7	<u>90.3</u>	81.2	20.3	0.6	94.1	87.3
035_power_drill	72.8	55.1	18.8	1.3	92.3	85.5	42.3	0.7	<u>84.2</u>	61.9
040_large_marker	71.4	58.0	20.7	8.4	86.2	75.6	<u>82.5</u>	51.9	80.0	64.3
MEAN	80.4	62.4	63.3	36.8	92.0	83.9	64.3	23.1	<u>85.7</u>	72.2

still achieve slightly higher accuracy due to large-scale training, GNC-Pose remains strikingly competitive—achieving comparable performance without using any learned features, training data, or category-specific priors. Specifically, ours outperforms prior template-based methods by a large margin, achieving 85.7% ADD-S and 72.2% ADD on average, compared to 64.3% / 23.1% for TP-UB. Remarkably, our learning-free pipeline even surpasses supervised baselines such as PoseCNN on both ADD-S (+5.3%) and ADD (+9.8%). The improvement is consistent across almost all objects, with particularly strong gains on challenging instances such as *010_potted_meat_can*, *005_tomato_soup_can*, *006_mustard_bottle*, and *021_bleach_cleanser*. These results demonstrate that geometry-aware correspondence filtering combined with GNC-PnP refinement provides a highly robust learning-free solution for 6D object pose estimation.

5 Ablation Studies

5.1 Setup

To better understand the contribution of each component in GNC-Pose, we conduct ablation studies on two representative YCB objects: *001_chips_can* and *004_sugar_box*. The chips can is approximately cylindrical with partial texture and strong rotational symmetry around its main axis, while the sugar box is relatively smaller and has more non-symmetric texture. For the Variations, We first ablate the proposed geometry-aware clustering and voxel-based weighting, replacing the per-point geometry weights with uniform weights $w_i^{\text{geom}} \equiv 1$. Next, we examine the impact of the GNC-based PnP refinement by comparing it against a classic Ransac PnP.

We report results in terms of ADDS AUC, ADD AUC at $0.1d$ and ADDS, ADD at $0.1d$.

Table 2. Ablation of geometry-aware weighting on YCB objects. Each entry reports: ADD AUC (0.1d) / ADD-S AUC (0.1d) / ADD < 0.1d (%) / ADD-S < 0.1d (%).

Variant	001_chips_can				004_sugar_box			
	ADD AUC (0.1d) / ADD-S AUC (0.1d) / ADD < 0.1d (%) / ADD-S < 0.1d (%)							
w/o geometry-aware weights	43.0	75.7	71.7	96.7	21.5	30.9	34.2	41.7
w/o GNC refinement	40.4	76.1	68.3	100	24.6	32.7	39.2	41.7
Full (ours)	44.1	78.0	65.1	100	31.9	41.7	48.3	52.5

5.2 Analysis

As shown in Table. 2, removing the geometry-aware weighting consistently degrades performance on both objects. For *004_sugar_box*, all the evaluation score drops noticeably when all correspondences are treated uniformly, indicating that many matches fall on geometrically ambiguous surfaces. The voxel-support density effectively suppresses these unstable regions and directs the optimization toward more discriminative structures such as edges and label boundaries. For *001_chips_can*, geometry-aware weighting also yields a clear improvement, suggesting enhanced stability in the final refinement stage.

Both objects likewise benefit substantially from the graduated non-convexity (GNC) block. On the sugar box, GNC block markedly increases robustness to outliers stemming from complex textures and imperfect feature matches along the box body. On the chips can, the effect is less pronounced—largely because the initial correspondences are already of high quality—but still provides a measurable improvement. By gradually tightening the effective inlier set through the annealing of μ , the optimizer avoids being influenced by early noisy correspondences and converges to a more stable solution.

6 Conclusions

We presented GNC-Pose, a fully learning-free framework for monocular 6D object pose estimation on textured objects. The pipeline begins with multi-view rendering to establish dense correspondences, incorporates geometry-aware weighting to suppress ambiguous matches, and employs a non-convex GNC-based PnP solver for robust optimization. By combining structural priors derived directly from the CAD model with a principled graduated non-convexity schedule, our method achieves stable convergence under severe correspondence noise and geometric ambiguity—without relying on learned features, annotated datasets, or category-specific priors. Extensive experiments on the YCB Object and Model Set [4] show that GNC-Pose substantially outperforms existing learning-free approaches and achieves accuracy competitive with modern learned systems, while remaining lightweight and CPU-efficient.

Looking ahead, we plan to incorporate object tracking, extend the method to deformable and articulated objects, and leverage temporal priors for real-time robotic manipulation. Another promising direction is to tackle strongly textureless or low-contrast objects by integrating geometry-aware priors with

differentiable rendering or photometric consistency cues, enabling reliable pose estimation even when appearance-based features become uninformative.

References

1. Agarwal, S., Mierle, K., et al.: Ceres solver: Tutorial & reference. Google Inc **2**(72), 8 (2012)
2. Besl, P.J., McKay, N.D.: Method for registration of 3-d shapes. In: Sensor fusion IV: control paradigms and data structures. vol. 1611, pp. 586–606. Spie (1992)
3. Bhattacharjee, S.: Dls and zeta potential—what they are and what they are not? *Journal of controlled release* **235**, 337–351 (2016)
4. Calli, B., Singh, A., Walsman, A., Srinivasa, S., Abbeel, P., Dollar, A.M.: The ycb object and model set: Towards common benchmarks for manipulation research. In: 2015 international conference on advanced robotics (ICAR). pp. 510–517. IEEE (2015)
5. Deng, W., Campbell, D., Sun, C., Zhang, J., Kanitkar, S., Shaffer, M.E., Gould, S.: Pos3r: 6d pose estimation for unseen objects made easy. In: Proceedings of the Computer Vision and Pattern Recognition Conference. pp. 16818–16828 (2025)
6. Di, Y., Manhardt, F., Wang, G., Ji, X., Navab, N., Tombari, F.: So-pose: Exploiting self-occlusion for direct 6d pose estimation. In: Proceedings of the IEEE/CVF International Conference on Computer Vision. pp. 12396–12405 (2021)
7. Fischler, M.A., Bolles, R.C.: Random sample consensus: a paradigm for model fitting with applications to image analysis and automated cartography. *Communications of the ACM* **24**(6), 381–395 (1981)
8. Gu, C., Ren, X.: Discriminative mixture-of-templates for viewpoint classification. In: European Conference on Computer Vision. pp. 408–421. Springer (2010)
9. Haugaard, R.L., Buch, A.G.: Surfemb: Dense and continuous correspondence distributions for object pose estimation with learnt surface embeddings. In: Proceedings of the IEEE/CVF Conference on Computer Vision and Pattern Recognition. pp. 6749–6758 (2022)
10. He, Y., Wang, Y., Fan, H., Sun, J., Chen, Q.: Fs6d: Few-shot 6d pose estimation of novel objects. In: Proceedings of the IEEE/CVF Conference on Computer Vision and Pattern Recognition. pp. 6814–6824 (2022)
11. Hess, R.: An open-source siftlibrary. In: Proceedings of the 18th ACM international conference on Multimedia. pp. 1493–1496 (2010)
12. Hinterstoisser, S., Cagniart, C., Ilic, S., Sturm, P., Navab, N., Fua, P., Lepetit, V.: Gradient response maps for real-time detection of textureless objects. *IEEE transactions on pattern analysis and machine intelligence* **34**(5), 876–888 (2011)
13. Hinterstoisser, S., Lepetit, V., Ilic, S., Holzer, S., Bradski, G., Konolige, K., Navab, N.: Model based training, detection and pose estimation of texture-less 3d objects in heavily cluttered scenes. In: Asian conference on computer vision. pp. 548–562. Springer (2012)
14. Holland, P.W., Welsch, R.E.: Robust regression using iteratively reweighted least-squares. *Communications in Statistics-theory and Methods* **6**(9), 813–827 (1977)
15. Iwase, S., Liu, X., Khirodkar, R., Yokota, R., Kitani, K.M.: Repose: Fast 6d object pose refinement via deep texture rendering. In: Proceedings of the IEEE/CVF International Conference on Computer Vision. pp. 3303–3312 (2021)
16. Kuchlbauer, M., Liers, F., Stingl, M.: Adaptive bundle methods for nonlinear robust optimization. *INFORMS Journal on Computing* **34**(4), 2106–2124 (2022)

17. Labbé, Y., Carpentier, J., Aubry, M., Sivic, J.: Cosypose: Consistent multi-view multi-object 6d pose estimation. In: European Conference on Computer Vision. pp. 574–591. Springer (2020)
18. Lepetit, V., Moreno-Noguer, F., Fua, P.: Ep n p: An accurate o (n) solution to the p n p problem. *International journal of computer vision* **81**(2), 155–166 (2009)
19. Levenberg, K.: A method for the solution of certain non-linear problems in least squares. *Quarterly of applied mathematics* **2**(2), 164–168 (1944)
20. Li, J., Miller, A.H., Chopra, S., Ranzato, M., Weston, J.: Learning through dialogue interactions by asking questions. *arXiv preprint arXiv:1612.04936* (2016)
21. Li, S., Xu, C., Xie, M.: A robust o (n) solution to the perspective-n-point problem. *IEEE transactions on pattern analysis and machine intelligence* **34**(7), 1444–1450 (2012)
22. Li, Y., Wang, G., Ji, X., Xiang, Y., Fox, D.: Deepim: Deep iterative matching for 6d pose estimation. In: Proceedings of the European conference on computer vision (ECCV). pp. 683–698 (2018)
23. Li, Z., Wang, G., Ji, X.: Cdpn: Coordinates-based disentangled pose network for real-time rgb-based 6-dof object pose estimation. In: Proceedings of the IEEE/CVF international conference on computer vision. pp. 7678–7687 (2019)
24. Peng, S., Liu, Y., Huang, Q., Zhou, X., Bao, H.: Pvnnet: Pixel-wise voting network for 6dof pose estimation. In: Proceedings of the IEEE/CVF conference on computer vision and pattern recognition. pp. 4561–4570 (2019)
25. Rublee, E., Rabaud, V., Konolige, K., Bradski, G.: Orb: An efficient alternative to sift or surf. In: 2011 International conference on computer vision. pp. 2564–2571. Ieee (2011)
26. Sun, J., Shen, Z., Wang, Y., Bao, H., Zhou, X.: Loftr: Detector-free local feature matching with transformers. In: Proceedings of the IEEE/CVF conference on computer vision and pattern recognition. pp. 8922–8931 (2021)
27. Sünderhauf, N., Protzel, P.: Switchable constraints for robust pose graph slam. In: 2012 IEEE/RSJ International Conference on Intelligent Robots and Systems. pp. 1879–1884. IEEE (2012)
28. Tian, Y., How, J.P.: Spectral sparsification for communication-efficient collaborative rotation and translation estimation. *IEEE Transactions on Robotics* **40**, 257–276 (2023)
29. Wang, G., Manhardt, F., Tombari, F., Ji, X.: Gdr-net: Geometry-guided direct regression network for monocular 6d object pose estimation. In: Proceedings of the IEEE/CVF conference on computer vision and pattern recognition. pp. 16611–16621 (2021)
30. Wen, B., Yang, W., Kautz, J., Birchfield, S.: Foundationpose: Unified 6d pose estimation and tracking of novel objects. In: Proceedings of the IEEE/CVF Conference on Computer Vision and Pattern Recognition. pp. 17868–17879 (2024)
31. Xiang, Y., Schmidt, T., Narayanan, V., Fox, D.: Posecnn: A convolutional neural network for 6d object pose estimation in cluttered scenes. *arXiv preprint arXiv:1711.00199* (2017)
32. Xiao, G., Ma, J., Wang, S., Chen, C.: Deterministic model fitting by local-neighbor preservation and global-residual optimization. *IEEE Transactions on Image Processing* **29**, 8988–9001 (2020)
33. Yang, H., Antonante, P., Tzoumas, V., Carlone, L.: Graduated non-convexity for robust spatial perception: From non-minimal solvers to global outlier rejection. *IEEE Robotics and Automation Letters* **5**(2), 1127–1134 (2020)

- 34. Yang, H., Carlone, L.: One ring to rule them all: Certifiably robust geometric perception with outliers. *Advances in neural information processing systems* **33**, 18846–18859 (2020)
- 35. Yang, H., Shi, J., Carlone, L.: Teaser: Fast and certifiable point cloud registration. *IEEE Transactions on Robotics* **37**(2), 314–333 (2020)
- 36. Zhao, J., Xu, W., Kneip, L.: A certifiably globally optimal solution to generalized essential matrix estimation. In: *Proceedings of the IEEE/CVF Conference on Computer Vision and Pattern Recognition*. pp. 12034–12043 (2020)